Separated Flow Upstream of a Jet in a Crossflow

A. Krothapalli* and L. Lourenco†
FAMU/FSU College of Engineering, Tallahassee, Florida
and
J. M. Buchlin‡
Von Kármán Institute for Fluid Dynamics, Rhode-St.-Genese, Belgium

The complex flow in the recirculation region upstream of a rectangular jet issuing normally into a uniform crossflow has been examined using flow visualization techniques. The variation of the primary separation distance with velocity ratio revealed the existence of two different flow regimes. The change from one to the other occurs at a velocity ratio of 5. The recirculation region upstream of the jet is found to be unsteady and periodic. The frequency of this periodic motion appears to be the same as that produced by the vortex shedding in the near wake. Depending upon the flow parameters, the wake behind the jet displays two distinct vortical structures, one dominated by a symmetric vortex pair, forming a closed region, and the other with vortices shed alternately from each side of the jet, similar in nature to the flow past solid bluff bodies. It is also shown that the Strouhal number based on the vortex shedding frequency varies uniquely with the velocity ratio

I. Introduction

THE problem addressed here is the experimental determination of the separated flow structure upstream of a subsonic rectangular jet issuing from a flat plate into a uniform oncoming subsonic freestream. This investigation is prompted by the interest in short takeoff and vertical landing (STOVL) aircraft configurations that utilize rectangular jets issuing normal to the wing for powered lift. Such a jet could be produced by installing a two-dimensional ejector along the span of the wing.

The classical jet in a crossflow problem has been well researched by many investigators. The focus of these investigations has been mainly on the determination of the jet structure and its induced pressures on the body from which it issues. Several review articles[1-3] describing the jet-induced effects have appeared in the literature; thus, no attempt is made here to discuss the previous work. However, the separated flow region upstream of the jet near the nozzle exit is presently least understood. For example, in early investigations the unsteady nature of the separated flow region, which is dominated by a horseshoe-type vortex flow, was not studied.

Another aspect of this problem is the vortex shedding associated with the wake flow behind the jet. The frequency of this vortex shedding received some attention in the literature, and the early references are given in McMahon et al.[4] For the measurement of shedding frequency McMahon et al.[4] used an experimental configuration similar to the present work. In their experiments the freestream Reynolds number about 10^6. The data show that the shedding frequency was nondimensionalized using the breadth of the jet and the freestream velocity is about 0.1 for a velocity ratio (mean jet exit velocity/mean freestream velocity) of 8 and remains unchanged with increasing velocity ratio. Using flow visualization techniques, McAllister[5] studied the vortex shedding phenomenon behind a circular water jet in a crossflow in a water tunnel. The data show that the nondimensional shedding frequency based on jet exit diameter varied with velocity ratio from $St = 0.103$ for $V_j/V_\infty = 3.83$ to $St = 0.019$ at $V_j/V_\infty = 34$ for a relatively small range of Reynolds numbers (based on the jet exit diameter and freestream velocity) of 2000 to 6000. A similar observation was also made by Moussa et al.[6] At present, data based on symmetric experiments at high Reynolds numbers and in the range of velocity ratios of practical interest is not available.

The main parameters governing the flow field are the Reynolds number and Mach number of the jet and the freestream, the velocity profile and the disturbance characteristics at the jet exit, the nature of the disposition of the jet, and the boundary-layer characteristics upstream of the nozzle exit. In the present experiment the jet is issued normally into the freestream. Its Reynolds number, based on the nozzle width, is varied from 6×10^3 to 10^5, its freestream Reynolds number, based on the jet disposition length (the distance between the leading edge of the flat plate and the jet exit), is varied from 5×10^4 to 5×10^6, and the aspect ratio of the rectangular nozzle is varied from 6 to 10. A turbulent boundary layer was maintained upstream of the nozzle exit. The principal goal of this experiment is to understand the main physical features of the upstream separated flow at the nozzle exit and obtain satisfactory relations between the flow characteristics and the many parameters governing them.

II. Apparatus, Instrumentation, and Procedures

The experiments were carried out in two different facilities and locations. Most of the experiments were conducted in the close return subsonic wind tunnel at The Florida State University. This facility has a test section 0.6 m wide, 0.6 m high, and 1.5 m long, and its freestream velocity ranges from 1 m/s to 70 m/s. For the range of freestream velocities considered, the freestream turbulence level is less than about 0.5%. The second facility is a close return subsonic wind tunnel at Von Karman Institute (VKI) in Belgium. The test section is 0.35 m wide, 0.35 m high, and 1 m long. In this wind tunnel the freestream velocity can be varied from 1 m/s to 15 m/s. The

Received Nov. 1, 1988; presented as Paper 89-0571 at the AIAA 27th Aerospace Sciences Meeting, Reno, NV, Jan. 9–12, 1989; revision received March 1, 1989.

*Professor and Chairman, Department of Mechanical Engineering. Member AIAA.
†Associate Professor, Department of Mechanical Engineering. Member AIAA.
‡Professor. Member AIAA.

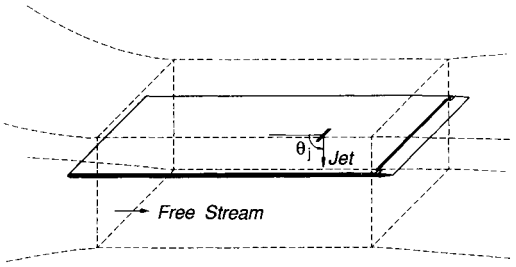

Fig. 1 A schematic of the experimental arrangement.

test conditions established during these experiments and their corresponding nondimensional parameters are as follows:

$$1 \text{ m/s} < V_\infty < 60 \text{ m/s}$$

$$10 \text{ m/s} < V_j < 120 \text{ m/s}$$

$$5 \times 10^4 < RE_\infty < 5 \times 10^6$$

$$6 \times 10^3 < Re_j < 10^5$$

$$1.0 < \frac{V_j}{V_\infty} < 14$$

where V_∞ is the mean freestream velocity, V_j is the mean jet exit velocity, Re_∞ is the freestream Reynolds number based on the jet disposition length, and Re_j is the jet Reynolds number based on the width ($W = 0.01$ m) of the nozzle exit. The velocity ratio, if strictly defined, must be the square root of the jet to the freestream momentum flux. The velocities considered here are such that compressibility effects can be neglected: e.g., for the highest velocities considered, 120 m/s for the jet flow and 40 m/sec for the freestream. The correction to the velocity ratio due to compressibility effects is about 3%. Hence, for the data presented here, the velocity ratio is defined simply as V_j/V_∞. The mean temperatures of the jet and the freestream were constant and kept at 300 °K.

A 2.5-cm-thick plexiglas flat plate 0.6 m wide and 1.5 m long was installed in the test section as shown in Fig. 1. The plate was rigidly mounted 0.2 m from the top wall of the test section with six streamlined supports having NACA 0018 airfoil cross sections with 0.063-m chord. The flat plate was fitted with a variable angle of attack flap that is used to adjust the pressure gradient on the plate. A 2.5-cm-wide boundary-layer trip, made of 20-μm-diameter glass beads, was placed 5 cm downstream of an elliptic (2.5:1) leading edge. The nozzle exit was positioned in the center of the plate, 1.17 m downstream of the leading edge. A nozzle assembly fit flush with the plate surface and the top wall of the test section. The nozzle assembly is shown in Fig. 2. Pairs of nozzle blocks were used to change the long dimension of the nozzle, thus achieving several different aspect ratios. The width of the nozzle exit was kept constant at 1 cm. Without the presence of the jet, the pressure gradient on the plate was adjusted to be close to zero.

A similar experimental setup was also used at the VKI. The flat plate was 0.28 m wide and 0.86 m long. The nozzle exit was located 0.56 m downstream of the leading edge, and the boundary layer was not tripped in these experiments.

Three different flow visualization techniques were used to obtain the main features of the separated flowfield: the surface oil flow technique using TiO_2, smoke flow visualization by a laser sheet, and an infrared thermographic technique. The infrared thermographic technique provided the surface temperature distribution on the flat plate, which was heated with a constant heat flux. It is shown that the surface temperature field maps the separated flow regions distinctly.

In order to obtain a constant surface heat flux for use with the infrared thermographic technique, two heater plates

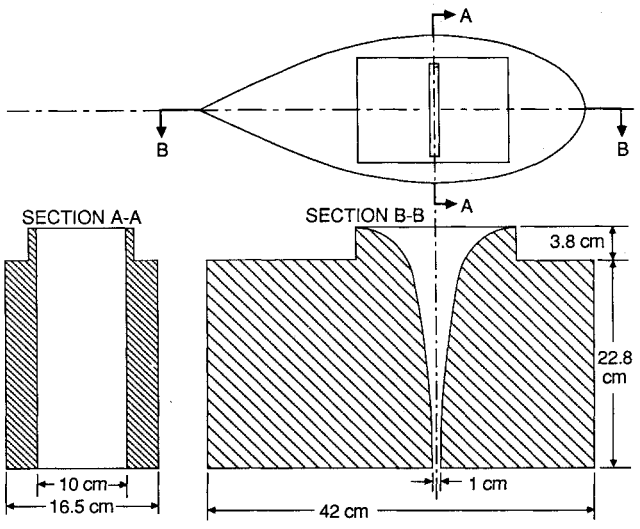

Fig. 2 The details of the nozzle assembly.

56 × 60 cm and 56 × 45 cm) were flush mounted into a recessed part of the Plexiglas plate near the nozzle exit. The steady-state temperature, which was uniform in the region of interest, never exceeded 36°C, thus minimizing thermal effects on the overall flowfield. This setup was used for surface flow visualization purposes only and no attempt was made to study the heat-transfer properties of the flowfield. The detailed calibration procedure and manufacturing of the constant heat flux source plates are discussed by Gladnick and Buchlin.[7] The infrared camera used was an Inframetrics mode 600. The real time images were captured on a video tape and processed at a later time. The unsteady nature of the separated region was investigated using standard hot-wire anemometry and associated electronics.

It is perhaps appropriate at this stage to emphasize that no attempt was made in the present work to study the jet structure, nor the detailed boundary-layer structure ahead of the jet. However, some boundary-layer measurements were made using a standard boundary-layer pitot tube to obtain the global properties of the boundary layer upstream of the jet exit. Similarly, using a standard pitot-static tube, the mean exit velocity of the jet was measured and found to be uniform with a top hat profile. The detailed nature of the boundary layers at the nozzle exit cannot, however, be discerned from these measurements.

The overall phenomena inherent to the flow near the jet exit could be considered at this stage of our knowledge free of any direct influence from the blockage of the test section by the jet or due to jet impingement. For example, at a velocity ratio of 15, the jet centerline meets the bottom wall of the wind tunnel about 1 m downstream of the jet exit, the location of which is well beyond the test section. Except at very high velocity ratios (greater than about 20), the jet does not impinge on the bottom wall of the test section.

III. Results and Discussion

In the following section, some selected data will be presented and discussed, and an effort is made to restrict the presentation to only those results that are pertinent to the discussion. General conclusions and recommendations are made in Sec. IV.

A. Upstream Flow Structure

A typical oil visualization picture of the surface flow near the nozzle exit is shown in Fig. 3. In this picture, the direction of the freestream is indicated by the arrow. The corresponding mean freestream and jet exit velocities and the velocity ratio are 40 m/s, 120 m/s, and 3, respectively. The freestream

Reynolds number based on the jet disposition length of 1.17 m is 3.12×10^6, and the jet Reynolds number based on the nozzle width is about 0.8×10^5. The undisturbed boundary layer just ahead of the nozzle exit is found to be turbulent with a thickness, based on $0.99V_\infty$, of about 2 cm. This surface flow picture shows remarkable details of the separated region ahead of the jet and the near wake region behind the jet. The main features of this flow are the two well-defined regions, the region of attached flow and the region of separated flow marked by the primary separation line. A secondary separation line is observed between the jet exit and the primary separation line. These separation lines are the signature of a horseshoe-type vortex system. The signature of the twin tornado-like vortices that rise up from the near wake can also be seen in this picture. A similar structure is also observed at other velocity ratios, except that the distinction between the primary and secondary separation lines becomes less discernible at low (say $V_j/V_\infty < 1.5$) and high ($V_j/V_\infty > 8$) velocity ratios.

A typical instantaneous laser sheet visualization picture, using smoke as seeding material, of a low Reynolds number flow in the central plane normal to the jet exit, or sideview, is shown in Fig. 4. This picture is obtained from a single-frame video recording. The directions of the jet and freestream are indicated by the arrows. The corresponding velocity ratio is about 2.5. In this frame the main feature is the existence of two separate vortices rotating in clockwise direction. However, most of the frames show the presence of a single large vortex with varying location. Although the flow in the vertical central plane seems to be unsteady, the surface flow signature obtained over a long period of time (about 5 min) in the plane view displays an organized horseshoe-type vortex structure as shown in Fig. 3.

These and other real-time observations suggest that the formation and rollup of these vortices in the recirculation region is a time-dependent periodic phenomenon. For instance, measurements at a velocity ratio of 2.5 display a periodicity with a frequency of about 2 Hz. This frequency seems to be related to the vortex shedding behind the jet. This aspect is discussed later.

Based on the analysis of several surface flow visualization and laser sheet visualization pictures in the plane of symmetry, a multiple vortex structure is proposed. This structure is schematically depicted in Fig. 5. Although difficult to discern, the photographs indicate the attachment lines and are shown

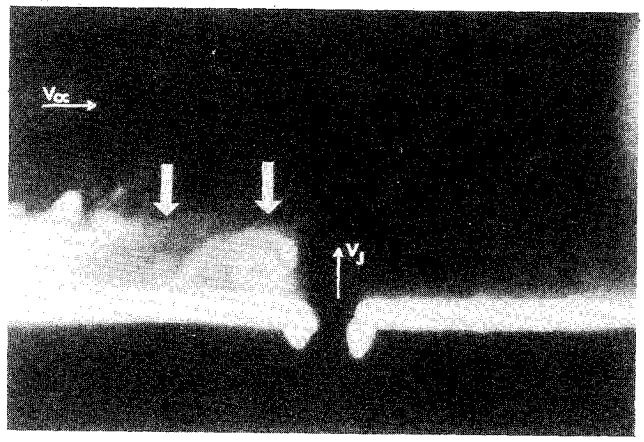

Fig. 4 A typical instantaneous laser sheet picture in the plane of symmetry. The arrows indicate two counter-rotating vortices. Velocity ratio = 2.5.

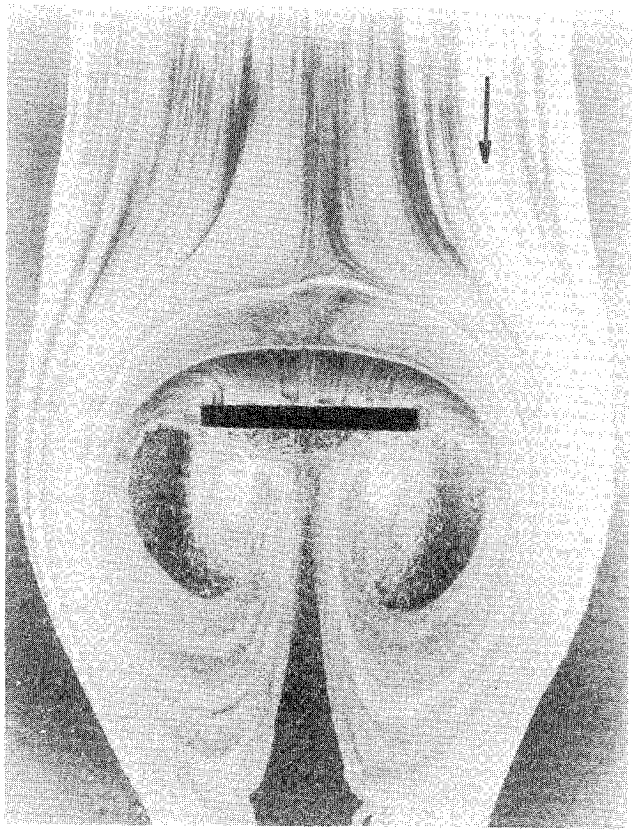

Fig. 3 A typical surface oil flow picture of the separated region. Velocity ratio = 3.0.

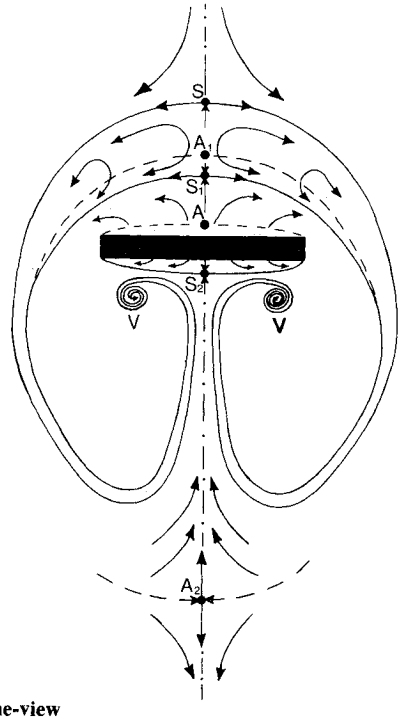

a) Plane-view

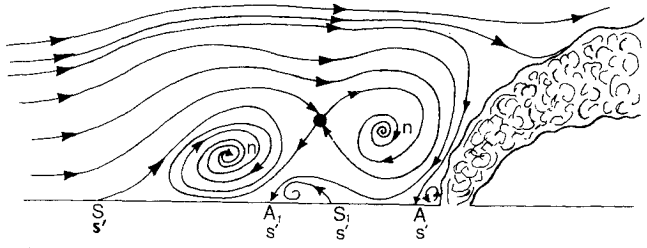

b) Side-view in the plane of symmetry

Fig. 5 A schematic of the separated flow region: S = primary separation; S_1 = secondary separation; A = attachment; V = vortex; n = node; s' = half-saddle.

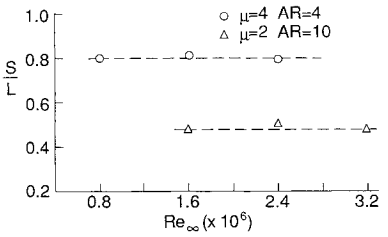

Fig. 6 The variation of the nondimensional separation distance with freestream Reynolds number.

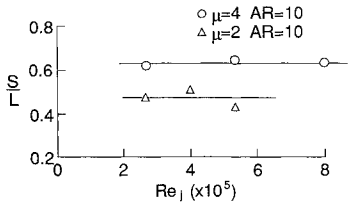

Fig. 7 The variation of the nondimensional separation distance with jet Reynolds number.

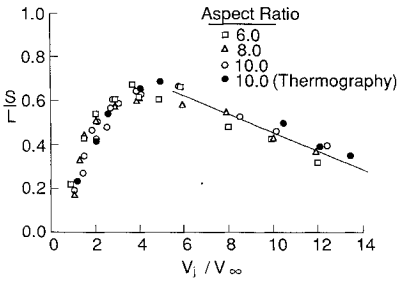

Fig. 8 The variation of the nondimensional separation distance with velocity ratio. The solid line is drawn to indicate the linear variation.

in Fig. 5a. These are supported by the known topological rules for steady separated flows.[8] The multiple vortex structure shown in Fig. 5b also follows these topological rules. The lines with arrow heads in Fig. 5a represent skin-friction lines that converge asymptotically to the line of separation. A similar vortex structure was also observed in three-dimensional separated flows created by an obstruction mounted on a flat plate.[9] The adverse pressure gradients and the deflection of streamlines due to the blockage effect of the jet cause the oncoming boundary layer to be separated and form this complicated vortex pattern. In the present experiment, this separation process is complicated by the jet entrainment effect and the upstream influence of the unsteady wake behind the jet.

One of the quantities of interest in the jet-crossflow interaction is the extent of the separated flow upstream of the jet. This boundary can be defined by the primary separation line. Since there is a plane of symmetry in the flow, the distance from the leading edge of the nozzle exit to the primary separation line S in the central plane can be used as an estimate of the extent of the separated region. The primary separation line is easily determined from plane view of oil flow pictures and by further infrared thermographic measurements. The accuracy of the measured values of S is, in most cases, $\pm 10\%$. The primary separation distance is a function of the following nondimensional parameters:

$$\frac{S}{L} = f(AR, Re_\infty, Re_j, \mu)$$

where Re_∞ is the freestream Reynolds number based on the jet disposition length and freestream velocity, Re_j is the jet

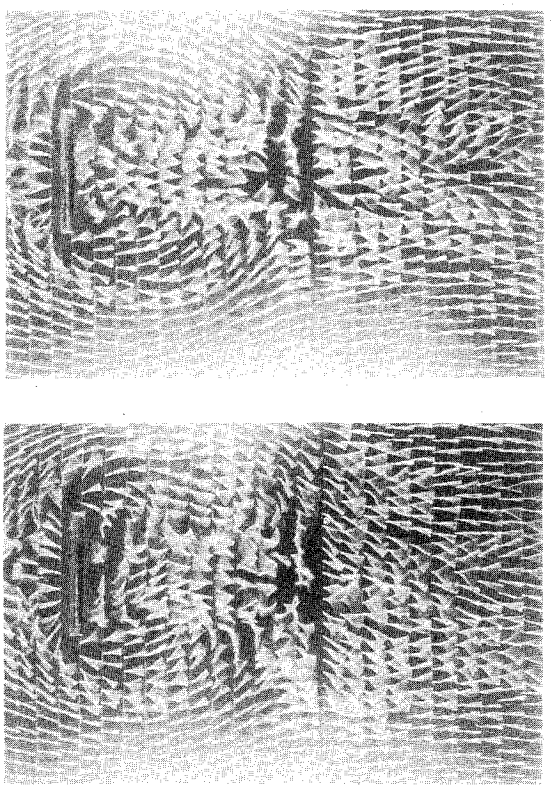

Fig. 9 The near wake structure of a weak jet at two different random times. Velocity ratio = 3.0.

Reynolds number based on the width of the nozzle exit and jet exit velocity, μ is the velocity ratio $= V_j/V_\infty$, and AR is the aspect ratio $= L/W$.

For the conditions tested, it was found that the separation distance did not vary with either the freestream Reynolds number or the jet Reynolds number as shown in Figs. 6 and 7. Thus, the separation distance becomes a function of the two remaining variables, namely, AR and μ.

Figure 8 shows the variation of S/L with the velocity ratio μ for three different aspect ratios. The separation distance obtained using the thermographic technique is also included in the figure. The trend of the data plotted in this manner shows two distinct regimes, the change from one to the other occurring at a velocity ratio of 5. In the first regime, as expected, the separation distance increases monotonically with increasing velocity ratio, which is indicative of the blockage effect of the freestream by the jet. For velocity ratios greater than 5, the separation distance decreases, almost linearly, with increasing velocity ratio. This behavior might be related to the relatively large entrainment caused by the jet. The effect of the entrainment flow is to lower the upstream adverse pressure gradient. However, no firm conclusions can be made before a more detailed examination of the flow in the vicinity of the jet is undertaken. The data in Fig. 8 also show that the effect of the aspect ratio on S/L is small compared to the other nondimensional parameter μ for the moderate aspect ratios tested.

B. Shed Vortex System

In order to visualize the flow structure in the wake region, minitufts were placed on the plate as shown in Fig. 9. Using a 35-mm camera, photographs were taken for selected velocity ratios in the range from 1.0 to 12. The photographs were taken at random and with an exposure time of 8×10^{-3} s. Examination of the photographs revealed the presence of two different types of flow structure in the wake region as shown in Figs. 9 and 10. Figure 9 presents two randomly selected photographs of the wake for a velocity ratio of 3.0

($V_j = 120$ m/s, $V_\infty = 40$ m/s). The near wake structure shows a symmetrical pair of vortices comparable to that observed behind a bluff body with an appropriately positioned splitter plate or base bleeding.[11] Such a vortex pair is observed only in the range of velocity ratios from 1 to about 5. In this range the length of the recirculation region is observed to grow in the flow direction with increasing velocity ratio. For example, the length of this region is about $1.6L$, where L is the breadth of the jet, for a velocity ratio of 2 and increases to $1.9L$ for a velocity ratio of 4. Note that contrary to pictures of symmetric vortices behind two-dimensional bluff bodies, here the symmetric vortices are not two-dimensional and the corresponding vortex lines spread upwards into the stream. A periodicity in the wake is observed, and the characteristic frequency seems to correlate well with frequencies measured at different velocity ratios as shown in Fig. 14. A quite different flow structure is observed when the velocity ratio is increased beyond a value of 5. A typical example of such a flow structure is shown in Fig. 10, which corresponds to a velocity ratio of 10 ($V_j = 120$ m/s, $V_\infty = 12$ m/s). These photographs reveal the presence of periodic asymmetric vortices with a flow structure similar to that behind a solid body.[12] This observation is consistent with that of McMahon et al.[4] behind a low–aspect ratio rectangular jet at a velocity ratio of 8. These two examples are representative of wake flow for a weak jet ($1.0 \leq \mu \leq 5$) and a strong jet ($\mu > 5$). Based on our surface flow visualization photographs we believe that for a weak jet the tornado-like vortices behind the jet are quite intense and the surrounding fluid is drawn up into the jet, thus creating a relatively low pressure in the near wake region, leading to the formation of the vortex pair as shown in Fig. 9. However, when the velocity ratio is increased beyond a value of 5, the tornado-like vortices move away from each other and become relatively weak, thus minimizing their influence on the shed vortices. A better understanding of the nature of near wake flowfield is left for future investigations.

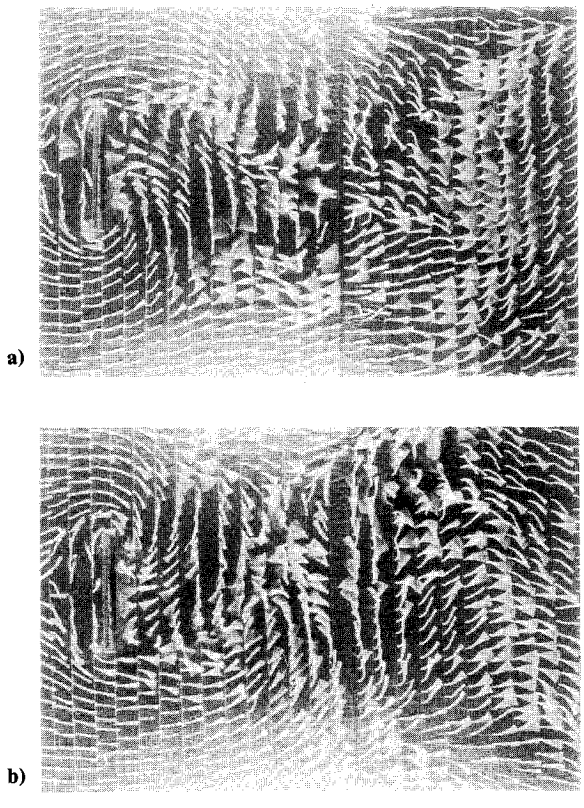

Fig. 10 The near wake structure of strong jet at two different random times. Velocity ratio = 10.0.

C. Unsteady Nature of the Recirculation Region

To further explore the periodic behavior of the flow, hot-wire anemometry was used primarily for the measurement of the frequency spectra of the velocity fluctuations both upstream and downstream of the nozzle exit. Hot-wire traverses around the jet indicate that the periodicity of the flow ahead of and behind the jet becomes weaker with increasing distance from the plate. At about 3 cm away from the plate a dominant frequency of the periodicity is clearly observed. Hence, this position was chosen for most of the measurements.

Figures 11a and 11b show the frequency spectra of the velocity fluctuations at selected positions downstream and upstream of the jet exit, respectively. The velocity ratio corresponding to these spectra is 1.6 ($U_j = 57$ m/s, $U_\infty = 35$ m/s). The positions of the hot-wire probe are indicated by a small circle and are drawn to scale with respect to the nozzle. These spectra are portions of power spectra that are obtained in the frequency range between 0 and 50 Hz, with a bandwidth of 1.45 Hz. However, an accurate reading of 0.5 Hz of the

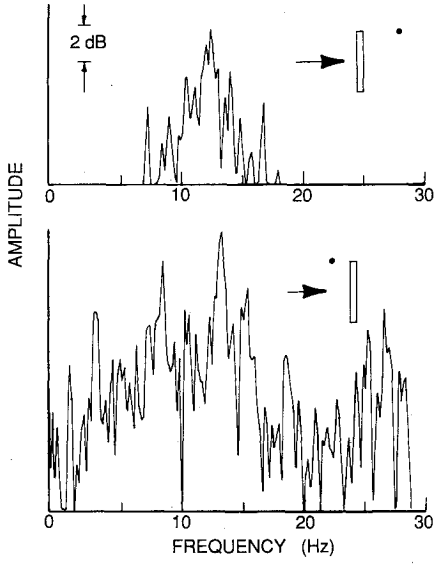

Fig. 11 Typical spectra of hot-wire signals for a weak jet: a) downstream of the jet exit; b) upstream of the jet exit. The closed circle indicates the position of the probe. Velocity ratio = 1.6.

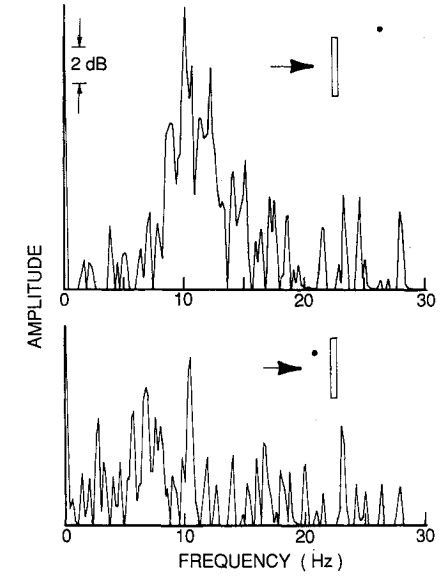

Fig. 12 Typical spectra of hot-wire signals for a strong jet: a) downstream of the jet exit; b) upstream of the jet exit. Velocity ratio = 6.6.

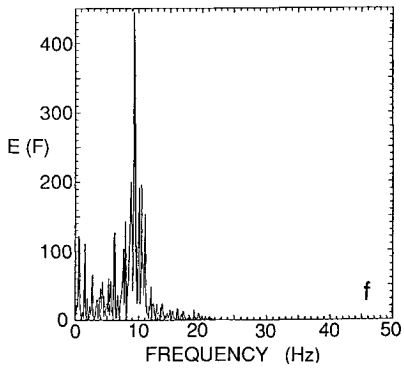

Fig. 13 A typical spectrum of the hot-wire signal in the near wake of a strong jet. Velocity ratio = 11.5.

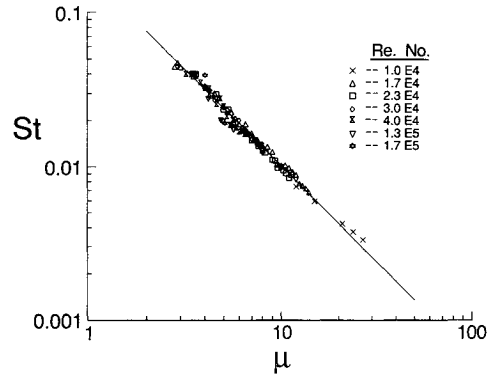

Fig. 14 The variation of the near wake Strouhal number with velocity ratio for different freestream Reynolds numbers.

frequency corresponding to any spectral peak can easily be obtained. A group of prominent peaks or a prominent peak accompanied by side peaks are apparent in these spectra. This is similar to the spectra observed in the wake of a finite circular cylinder at corresponding Reynolds numbers.[10] The important fact to note is that a dominant peak in the spectra of Fig. 11a corresponds to vortex shedding frequency of 14 Hz. While observing the spectra obtained at some distance ahead of the jet, as shown in Fig. 11b, it is apparent that a maximum amplitude peak exists at a frequency of 14.8 Hz. This peak has an amplitude of about 2 dB higher than the background. The proximity of the values of these frequencies leads us to believe that the unsteadiness observed in the flow visualization pictures in the recirculation zone ahead of the jet has a frequiency close to the vortex shedding frequency behind the jet. In order to confirm this finding, similar spectra are obtained at several momentum ratios. Figure 12 shows the spectra obtained in the near wake and in front of the jet at a relatively high momentum ratio. The velocity ratio corresponding to these spectra is 6.6 ($U_j = 67$ m/s; $U_\infty = 11$ m/s). It is found by observation that the location of the strongest hot-wire signal depends on the velocity ratio. The prominent peak in the wake is observed at 10 Hz, while in the recirculation zone ahead of the jet an amplitude dominant peak is observed at 10.8 Hz (see Fig. 12b). Similar observations are made in the entire range of momentum ratios considered in this experiment. From these observations we suggest that the periodicity in the recirculation zone ahead of the jet is the consequence of vortex shedding behind the jet. Although not demonstrated in this experiment, we believe that a splitter plate behind the jet, positioned appropriately, would not only inhibit the periodic vortex formation in the wake but would also minimize the unsteadiness in the upstream recirculation zone. Indeed, it has been shown[4] that the vortex shedding can be eliminated by placing a splitter plate behind the jet.

Now the dependence of the shedding frequency on velocity ratio and freestream Reynolds number is addressed. The shedding frequencies are measured by a hot-wire anemometer placed in the near wake. For most of the measurements, the hot-wire probe was placed 10 cm behind the jet and 6 cm above the plate. A typical spectrum of the hot-wire signal is shown in Fig. 13. The amplitude dominant frequency is referred to as the shedding frequency and is used in the calculation of the Strouhal number. It must, however, be noted that some variation, although not significant, of the frequency is observed when the hot wire is moved away from the plate. This variation is also observed for a finite cylinder[10] where the shedding frequency decreases gradually as one moves away from the plate.

In order to relate the variation of shedding frequency with the velocity ratio and freestream Reynolds numbers, previous investigators defined the Strouhal number based on the freestream velocity and characteristic length based on the nozzle breadth[4] or nozzle exit diameter for a circular jet.[6] The freestream Reynolds number is defined using the freestream velocity and the breadth of the jet. While attempting to analyze our data using the given definition for the Strouhal number (i.e., $St = fL/V_\infty$), it is found that the variation of St with μ shows significant scatter beyond the experimental uncertainty. For example, at a velocity ratio of 4, the magnitude of the Strouhal number varied from 0.1 to 0.15 in the range of freestream Reynolds number ($V_\infty L/\nu$) from 10,000 to 50,000. With increasing velocity ratio, this scatter is smaller, and the Strouhal number reaches an asymptotic value of about 0.1 for velocity ratios greater than 10. After careful examination of our data, it is clear that the given definition for the Strouhal number cannot be used for the entire range of velocity ratios and Reynolds numbers considered here. In contrast, when the Strouhal number is redefined in the following manner,

$$St = \frac{fL}{V_\infty (1+\mu^2)^{1/2}}$$

where a combination of freestream velocity and jet exit velocity is used, a significant reduction in the scatter is obtained as shown in Fig. 14. The data used here cover a broad range of velocity ratios, and the freestream Reynolds number varies from 10,000 to 170,000. The solid line shown in the figure corresponds to the following functional relationship:

$$St = 0.18\mu^{-1.25}$$

The results of McMahon et al.[4] are also in good agreement with the preceding correlation.

While there is a significant change in the near wake structure between weak and strong jets (Fig. 9 and 10), there is no apparent discontinuity in the variation of the Strouhal number with the velocity ratio (see Fig. 14). Hence, we conjecture that the basic mechanism for generation of the dominant frequency in the wake remains the same in both cases and that the change in the flow structure for a weak jet is related to upward (in the direction of the jet) rather than downstream covection of the vorticity.

IV. Conclusions

An understanding of the unsteady characteristics and the three-dimensional flow structure of the complex horseshoe vortical system in the upstream recirculation region is crucial for many engineering applications that utilize jets placed in a crossflow. However, the literature is quite sparse in documenting the fundamentals of the upstream separated flow structure.

In the present work an attempt is made to describe the basic structure of the separated recirculation region using known topological rules and flow visualization. The key elements of the flowfield are the presence of the horseshoe-type

vortices that are formed periodically with a frequency comparable to that of the vortex shedding behind the jet. The mean primary separation distance is found to be a function of the velocity ratio. This functional dependence depicts two distinct regimes, one dominated by the blockage effect of the freestream by the jet and the other by the entrainment process of the jet.

The flow structure in the wake shows two different types. The first one occurs for the case of a weak jet (i.e., $1 < \mu < 5$) and consists of a symmetric vortex pair forming a closed region. The other consists of vortices shedding alternately from each side of the jet quite similar to the flow past solid bluff bodies. This type of flow structure occurs in the case of a strong jet, (i.e., $\mu > 5$)). A unique functional relationship exists between the shedding frequency f expressed in dimensionless form in terms of the Strouhal number $St = fL/V_\infty\sqrt{1+\mu^2}$ and the velocity ratio. For the freestream Reynolds number tested ($10^4 < Re_\infty < 2 \times 10^5$), the relationship

$$St = \frac{0.18}{\mu^{1.25}}$$

is obtained by fitting the experimental data.

Acknowledgments

We would like to thank Mr. James Breeman, Mr. Ramesh Arjunji, and Mr. S. P. Gogineni for their assistance in the data gathering. Professor Chang Shih's comments have been helpful in our data analysis. We finally wish to express our gratitude to NASA Ames Research Center, Low Speed Aircraft Research Branch, for their financial support and patience.

References

[1]Kuhn, R. E., "The Induced Aerodynamics of Jet and Fan Powered V/STOL Aircraft," *Recent Advances in Aerodynamics*, Springer-Verlag, New York, 1986, pp. 337–373.

[2]Fearn, R. L., "Progress Towards a Model to Describe Jet/Aerodynamic–Surface Interference Effects," *Recent Advances in Aerodynamics*, Springer-Verlag, 1986, pp. 407–434.

[3]Margason, R. J., "Review of Propulsion Induced Effects on Aerodynamics of Jet V/STOL Aircraft," NASA TN D-5617, 1970.

[4]McMahon, H. M., Hester, D. D., and Palfrey, J. G., "Vortex Shedding from a Turbulent Jet in a Cross-wind," *Journal of Fluid Mechanics*, Vol. 48, 1971, pp. 73–80.

[5]McAllister, J. D., "A Momentum Theory of the Effects of Cross Flow on Incompressible Turbulent Jets," Ph.D. Dissertation, University of Tennessee, 1968.

[6]Moussa, Z. M., Trischka, J. W., and Eskinazi, S., "The Near Field in the Mixing of a Round Jet with a Cross Stream," *Journal of Fluid Mechanics*, Vol. 80, 1977, pp. 49–80.

[7]Gladnick, P. G. and Buchlin, J. M., "Experimental Examination Between a Cross Flowing Stream and Plane Jet on Localized Heat Transfer and Recirculation," Project Rept. 1986–11, Von Karman Institute for Fluid Dynamics, June 1986.

[8]Chapman, G. T., "Topological Classification of Flow Separation on Three-Dimensional Bodies," AIAA Paper 86-0485, Jan. 1986.

[9]Sedney, R. and Kitchens, C. W., "The Structure of Three Dimensional Separated Flows in Obstacle, Boundary Layer Interactions," *Flow Separation*, AGARD CP-168, May 1975, pp. 37.1–37.15.

[10]Ayoub, A. and Karamcheti, K., "An Experiment on the Flow Past a Finite Cylinder at High Subcritical and Supercritical Reynolds Numbers," *Journal of Fluid Mechanics*, Vol. 118, 1982, pp. 1–26.

[11]Berger, E. and Wille, R., "Periodic Flow Phenomena," *Annual Review of Fluid Mechanics*, Vol. 4, 1972, pp. 313–340.

[12]Cantwell, B. J., "A Flying Hot-wire Study of the Turbulent Near Wake of a Circular Cylinder at a Reynolds Number of 140,000," Ph.D. Thesis, California Inst. of Technology, Pasadena, CA, 1976.